Nuclear Instruments and Methods in Physics Research A 713 (2013) 5–10

Contents lists available at SciVerse ScienceDirect

Nuclear Instruments and Methods in Physics Research A

journal homepage: www.elsevier.com/locate/nima

Uncertainties in linear energy transfer spectra measured with track-etched detectors in space

Kateřina Pachnerová Brabcová [a,b,*], Iva Ambrožová [a], Zlata Kolísková [a,c], Alexandr Malušek [a,d]

[a] Department of Radiation Dosimetry, Nuclear Physics Institute, Academy of Sciences of Czech Republic, Na Truhlářce 39/64, 180 86 Praha, Czech Republic
[b] Nuclear Engineering, Department of Applied Physics, Chalmers University of Technology, SE-412 96, Göteborg, Sweden
[c] Faculty of Nuclear Sciences and Physical Engineering, Czech Technical University in Prague, Břehová 7, Czech Republic
[d] Radiation Physics, Department of Medical and Health Sciences, Linköping University, SE-581 85, Sweden

ARTICLE INFO

Article history:
Received 13 November 2012
Received in revised form
1 March 2013
Accepted 11 March 2013
Available online 18 March 2013

Keywords:
CR-39
Linear energy transfer
Uncertainty model
Space dosimetry

ABSTRACT

Polyallyldiglycol carbonate-based track-etched detectors can measure linear energy transfer (LET) spectra of charged particles. Accuracy of the spectra is affected by many factors whose effects are difficult to quantify. Typically, only uncertainty arising from the randomness of particle detection is reported in scientific literature. The aim of this paper is to classify the sources of uncertainties of an LET spectrum measurement and provide a simple model for the calculation of the combined uncertainty. The model was used for a spectrum measured with the track-etched detector (Harzlas TD-1) on board of the International Space Station from May–October 2009. For some spectrum bins the largest contribution to the combined uncertainty came from the uncertainty arising from the randomness of particle detection. For other bins it came from the uncertainty of the calibration curve. Contribution from the cross talk between bins was small for most of the bins as the width of the bins was relatively large compared to the intrinsic resolution of the track-etched detector. The analysis showed that sources of uncertainties other than the randomness of particle detection should not, in general, be neglected.

1. Introduction

Track-etched detectors (TEDs) have been used in dosimetry for more than 30 years. Their low price, small size and no build-in electronics make them useful especially for measurements on board spacecraft and aircraft [1,2]. Other applications of TEDs include radon monitoring [3], personal neutron dosimetry [4], nuclear fragmentation studies in radiation therapy [5], or detection of particles with very short ranges [6]. The detectors must be chemically or electrochemically processed to make particle tracks visible through a microscope. The number of etched particle tracks per unit detector area is then used to determine the fluence of detectable charged particles. If composition of the radiation field is known then this quantity can be used to estimate values of radiation protection quantities like absorbed dose or dose equivalent [7] via proper calibration factors. For an unknown radiation field, the radiation protection quantities can be determined from LET spectra of detected particles. Low-LET radiation like electrons and photons does not produce visible tracks in TEDs; typical LET thresholds for track creation are between 5 and 40 keV μm^{-1} depending on the detector material [8]. High-LET particles, which are a serious health concern in humans for their high ability to induce DNA damage [9], on the other hand create tracks whose sizes are related to the LET of passing particles [10].

LET spectra measured with TEDs are affected by uncertainties. Some uncertainties arise from limited knowledge about the composition of the radiation field, other from random effects during the calibration, etching, and signal read out of the detector. Determination of all these uncertainties is a difficult task. Several studies aimed at the determination of uncertainties associated with measurements of track diameters [11] or detection of fission fragments [12]. Most investigations focused on uncertainties associated with radon detection [13,14]. Their findings are not, however, directly applicable to LET spectrometry as uncertainties associated with detector calibration and response were not considered there. The aim of this paper is to classify the sources of uncertainties of an LET spectrum measurement and provide a simple model for the calculation of the combined uncertainty. Hitherto, an in-depth analysis of effects of individual factors affecting the accuracy of LET spectra measured with TEDs on board the International Space Station has not been published in scientific literature.

2. Theory

A heavy charged particle passing through a TED may create a latent track by changing the molecular structure of the original material. The latent track can be made visible through a

* Corresponding author at: Academy of Sciences of Czech Republic, Department of Radiation Dosimetry, Nuclear Physics Institute, Na Truhlářce 39/64, 180 86 Praha, Sweden. Tel.: +420 266 177 234; fax: +420 283 842 788.
E-mail addresses: brabcova@ujf.cas.cz, brabcova@chalmers.se (K. Pachnerová Brabcová), ambrozova@ujf.cas.cz (I. Ambrožová), koliskova@ujf.cas.cz (Z. Kolísková), alexandr.malusek@gmail.com (A. Malušek).

0168-9002/$ - see front matter © 2013 Elsevier B.V. All rights reserved.
http://dx.doi.org/10.1016/j.nima.2013.03.012

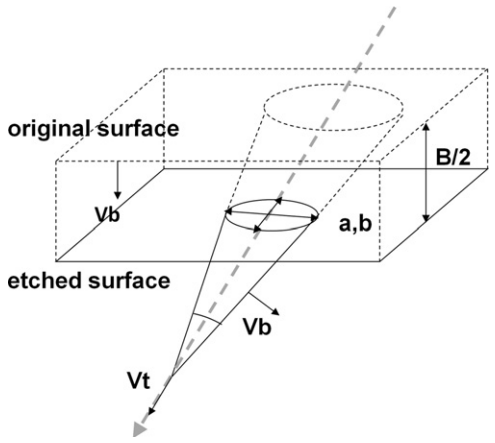

Fig. 1. Etching creates a conically shaped track whose intersection with the etched surface is an ellipse with major and minor axes a and b, respectively. The thickness of the removed layer on one side of the detector is $B/2$. Original trajectory of the heavy charged particle is visualised as a dashed line.

microscope by etching the detector in a suitable solution. The chemical process forms a conical-shape track as the track etch velocity, v_t, is typically larger than the surrounding material etch velocity, v_b. The etched track is then visible as a darker elliptical region on the surface of the detector foil. The etching velocity v_t can be determined from sizes of major and minor axes a and b, respectively, of the track ellipse [10] or length of the etched track [15], see Fig. 1.

The etching velocity v_b is defined as $v_b=(B/2)/t$, where t is the etching time and $B/2$ is the thickness of the removed layer from one side of the detector. The thickness B can be measured either directly [16], or indirectly [17]; a summary of all methods is in the review article by Nikezic and Yu [18]. In case of the indirect measurement, the thickness can be estimated for instance from radii of tracks created by perpendicularly impinging fission fragments of ^{252}Cf. The velocities v_t and v_b can be combined to a single dimensionless parameter $V=v_t/v_b$ called etch rate ratio. Durani and Bull [17] showed that the etch rate ratio V can also be calculated as

$$V=\left\{\text{sinarctan}\left[\frac{B}{2a}\left(1-\frac{b^2}{B^2}\right)\right]\right\}^{-1}, \tag{1}$$

where a and b are the major and minor axes, respectively, of the track ellipse, and B is the thickness of removed layer. It is assumed that B does not vary with position on the detector surface and thus is the same for all detected tracks. The etch rate ratio V depends on the linear energy transfer of the passing ionising particle [10]; this gives the detector spectrometric properties.

Eq. (1) is valid for conical tracks with $b<B$ and for time-independent track etch rate [15]; conical tracks with $b>B$ are handled in [18]. Tracks of particles with particle ranges shorter than the removed layer $B/2$ lose their conical shape and become rounded; these tracks are called over-etched. Shorter etching times and non-optical microscopy can be used to avoid over-etching [6].

Particles impinging on the detector in directions exceeding a so-called critical angle are not registered, as their tracks are either completely etched out or not elliptical. The critical angle depends on the LET of the particle and etching conditions [19]. A correction for the critical angle can be done by multiplying LET-spectrum bins by LET-specific correction factors.

2.1. Calibration curve

No generally applicable physical model describing the relation between the etch rate ratio V and the linear energy transfer L of the passing particle has been published so far. The relation, known as the calibration curve, is typically determined by fitting of suitable mathematical function of the form $V=f(L)$ to measured data and finding the inverse function $L=f^{-1}(V)$. High degree polynomial fits to data points $(L_i,\overline{V}_i)$, where $\overline{V}_i$ is an average of V taken over all tracks corresponding to the value of L_i, were often used in the past [15,20,21]. The inverse function can be calculated numerically or, for some functions, analytically [22].

Accuracy of the calibration curve is affected by factors like the non-homogeneity of detector material composition and thickness, concentration and temperature differences during etching, eventual residua after washing out of hydroxide, and performance of the operator who evaluates etched tracks. Uncertainties arising from random effects can, in principle, be estimated by repeating the experiment. In practice, however, this is difficult since awarded beam time at heavy ion accelerators is often quite limited and expensive. A common approach is to estimate the uncertainty using statistical properties of the fitting model. A known problem with uncertainties calculated this way is that they depend on the selection of the fitting model as the model itself puts some assumptions on distributions of fitted data.

2.2. Three-component model of uncertainty associated with an LET spectrum

Let $n_L(L)=dn/dL$ be the distribution of the mean number of tracks n within an area A of the detector surface with respect to the linear energy transfer L (shortly an "LET spectrum"), and let the LET spectrum be represented by a histogram. Then the mean number of tracks, Δn, in a bin with the LET of L_0 in the bin's centre is approximately.

$$\Delta n=n_L(L_0)\Delta L \tag{2}$$

where ΔL is the bin width. A measurement of Δn is affected by uncertainties. We propose a model where the uncertainty of Δn has three components: (i) uncertainty associated with randomness of particle detection, (ii) uncertainty arising from the uncertainty of the calibration curve, and (iii) uncertainty associated with detector response, which leads to a "crosstalk" between bins.

2.2.1. Uncertainty associated with randomness of particle detection

The number of tracks in a bin has a Poisson distribution, see e.g. [23]. The corresponding standard uncertainty, $u_1(\Delta n)$, is

$$u_1(\Delta n)=\sqrt{\Delta n} \tag{3}$$

2.2.2. Uncertainty arising from the uncertainty of the calibration curve

Values of the calibration curve $L=f^{-1}(V)$ are known with limited accuracy. A standard uncertainty $u(L)$ associated with the value of L taken from the calibration curve for a certain value of V propagates to an uncertainty, $u_2(\Delta n)$, associated with the expected number of tracks in a bin. Using the functional relationship (2) and the law of the propagation of uncertainty (Eq. A.1), the standard uncertainty $u_2(\Delta n)$ is

$$u_2(\Delta n)=\Delta L\left|\frac{dn_L}{dL}\right|u(L) \tag{4}$$

Note that the uncertainty is affected by the gradient of the LET spectrum. At regions where n_L as a function of L is approximately constant, the resulting $u_2(\Delta n)$ is almost zero.

2.2.3. Uncertainty associated with detector response

The response of a detector to particles with a specific value of L is not a single line in the LET spectrum; the original spectrum is smeared-out by a crosstalk between spectrum bins. The level of

Table 1
Nominal initial energy and LET at the target of heavy ions used for the detector calibration. Corresponding thickness of PMMA is also listed.

Ion, energy (MeV/u)	**LET** (**keV μm^{-1}**)	**PMMA** (**mm**)	**Detector**
C 290	13.06	0	D_1
	14.16	30.05	D_2
	15.89	63.26	D_3
C 135	23.53	0	D_4
	28.64	11.04	D_5
	36.05	18.47	D_6
C 400	10.85	0	D_7
	11.94	99.7	D_8
	18.76	207.51	D_9
Ne 400	31.23	0	D_{10}
	31.45	1.14	D_{11}
	32.86	20.78	D_{12}
Si 490	56.75	0	D_{13}
	61.3	60.95	D_{14}
	88.59	111.97	D_{15}
Fe 500	197.58	0	D_{16}
	232	30.05	D_{17}
	320	56.7	D_{18}

smear out can be described by a kernel $K(L,L')$ which gives the response of the detector as a function of L to particles with a specific value of L'. The measured spectrum $n_L(L)$ then depends on the original spectrum $n_L^*(L')$ as

$$n_L(L) = \int_L n_L^*(L')K(L,L')dL' \tag{5}$$

For example the kernel equation (6) smears out a single L' line to a Gaussian whose width depends on L' via the parameter $\sigma(L')$. The restoration of the original spectrum $n_L^*(L')$ from the measured spectrum $n_L(L)$ is a difficult task; spectrum lines which are significantly closer together than the bin width cannot be resolved and noise in bin counts may lead to a numerical instability in the solution. Since the original spectrum cannot be fully restored, the uncertainty, $u_3(\Delta n)$, associated with the detector response can be accurately estimated in certain situations only, for instance by modelling the original spectra and the resulting differences between bin counts of the original and smeared out spectra.

$$K(L,L') = \frac{1}{\sigma(L')\sqrt{2\pi}}\exp\left[-\frac{1}{2}\left(\frac{L-L'}{\sigma(L')}\right)^2\right] \tag{6}$$

2.2.4. The combined uncertainty

The presented model assumes that factors contributing to uncertainties $u_1(\Delta n)$, $u_2(\Delta n)$, and $u_3(\Delta n)$ described in previous sections are independent. Then covariances in Eq. (A.1) can be omitted and the combined uncertainty is calculated as

$$u_C(\Delta n) = \sqrt{u_1(\Delta n)^2 + u_2(\Delta n)^2 + u_3(\Delta n)^2} \tag{7}$$

3. Method

The model for the calculation of uncertainty described in Section 2 was applied on an LET spectrum measured in space. A polyallyldiglycol carbonate-based track-etched detector (commonly known as CR-39) manufactured by Fukuvi, Japan and distributed under the name Harzlas TD-1 was placed in the Piers-1 module section of International Space Station for 158 days from May 7th to October 11th, 2009. Processing of this detector, denoted as D_0, is described in Section 3.1. Calculation of the LET spectrum and associated uncertainties is in Section 3.4. Calibration curve was constructed from 18 Harzlas TD-1 detectors denoted as $D_1,\ldots,D_{18}$; the description is in Section 3.2. A separate experiment with 23 Harzlas TD-1 detectors denoted as $D_{19},\ldots,D_{41}$ was done to estimate the uncertainty of the removed layer B measurement when only (i) the randomness of the number and size of tracks produced by the spontaneous decay of ^{252}Cf, and (ii) the operator's performance were the affecting factors; the description is in Section 3.3.

3.1. Detector processing and readout

All detectors (D_0, $D_1,\ldots,D_{41}$) were etched in a 5 M solution of NaOH with the temperature of 70 °C for 18 h; the corresponding average etching velocity v_b was about 0.9 μm/h. Parameters a, b, and B of etched tracks were measured for a selected area of 0.06 cm^2 with the optic microscopic system HSP 1000 (SEIKO Precision INC) using the HspFit software [24]. Major and minor axes a and b, respectively, of each etched track were calculated by the HspFit software. The removed layer thickness, B, was estimated from radii of circular tracks created by heavier fission fragments of ^{252}Cf; irradiation with the ^{252}Cf source was done shortly before etching. The averages of B were calculated for each group etched in the same bath.

3.2. Calibration

The $D_1,\ldots,D_{18}$ detectors were perpendicularly irradiated with C^{6+}, Ne^{10+}, Si^{14+}, and Fe^{26+} heavy ion beams at the HIMAC-BIO facility [25] between 2008 and 2010. Each detector was irradiated in a separate accelerator run. LET of impinging ions was reduced using polymethyl methacrylate (PMMA) absorbers. Values of initial kinetic energy per unit mass and resulting LET, see Table 1, were provided by HIMAC staff; associated uncertainties were neglected. The provided LET values were in good agreement with values calculated using the SRIM code [26]. The detectors were processed and analysed using the method described in Section 3.1.

3.2.1. Expectations of V and associated uncertainties

Expectation $\overline{V}$ of the etch rate ratio was calculated from Eq. (A.2) using expectations $\overline{a}$, $\overline{b}$, and $\overline{B}$ specific for each detector $D_1,\ldots,D_{18}$; calculation of $\overline{a}$, $\overline{b}$, $\overline{B}$ and associated uncertainties $u(\overline{a})$, $u(\overline{b})$, $u(\overline{B})$ is in Sections 3.2.2 and 3.3. The uncertainty associated with $\overline{V}$ was calculated from the law of propagation of uncertainty Eq. (A.2) as

$$u_c^2(\overline{V}) = c_1^2u(\overline{a})^2 + c_2^2u(\overline{b})^2 + c_3^2u(\overline{B})^2 + 2c_1c_2u(\overline{a},\overline{b}) \tag{8}$$

There is no easy way to estimate the covariances $u(\overline{a},\overline{B})$ and $u(\overline{b},\overline{B})$; it was assumed that $u(\overline{a},\overline{B}) = u(\overline{b},\overline{B}) = 0$. This assumption overestimated the combined uncertainty in Eq. (8) since the products c_1c_3 and c_2c_3 were negative (see the Appendix).

Logarithmic transformations $\overline{\nu} = \lg(\overline{V})$and $\lambda = \lg(L/L_0)$, where $L_0 = 1$ keV μm^{-1}, were performed to make the data more evenly spaced for the regression analysis. The standard uncertainty $u(\overline{\nu})$ of the log-transformed variable was derived from the standard the uncertainty $u(\overline{V})$ of the measured data as [27]

$$u(\overline{\nu}) = \left|\frac{d\overline{\nu}}{d\overline{V}}\right| u(\overline{V}) = \frac{u(\overline{V})}{\overline{V}\ln 10} \tag{9}$$

Reciprocal values of $u^2(\overline{\nu})$ were used as statistical weights in the fitting model of the function $\nu = f(\lambda)$. A suitable fit was obtained with a third degree polynomial. To demonstrate that estimated uncertainties depend on the fitting model, a piecewise linear function was also used. The calibration curve $\lambda = f^{-1}(\nu)$ was obtained as the inverse function of $\nu = f(\lambda)$. The standard uncertainty associated with a value λ of the calibration curve (the accuracy of the calibration curve) was calculated from the

standard uncertainty $u(\nu)$ predicted by the linear regression model for the $\nu = f(\lambda)$ fit as [27]

$$u(\lambda) = \left|\frac{d\lambda}{d\nu}\right| u(\nu) = \left|\frac{df^{-1}(\nu)}{d\nu}\right| u(\nu) = \left|\frac{df(\lambda)}{d\lambda}\right|^{-1} u(\nu) \quad (10)$$

where the derivative $df/d\lambda$ was calculated analytically. The standard uncertainty $u(\nu)$ was taken as the difference between the predicted confidence limit and predicted expectation.

3.2.2. Expectations of a and b and associated uncertainties

Expectations $\bar{a}$ and $\bar{b}$, associated standard uncertainties $u(\bar{a})$ and $u(\bar{b})$, and the covariance $u(\bar{a},\bar{b})$ were calculated from tracks with $0.9 < b/a < 1$ and $b_{\min} < b < b_{\max}$. The ranges $b_{\min}$ and $b_{\max}$ were determined by visual inspection of Gaussian kernel density estimates of probability density functions; the interval was selected to cover the main peak of b values. This approach is demonstrated in Fig. 2, which shows a scatter plot of measured values a and b for all etched tracks with $b/a > 0.9$ and $5\,\mu m < b < 9\,\mu m$ created by 400 MeV/u carbon ions perpendicularly impinging on the TD-1 detector. Also shown is the Gaussian kernel density estimate of the probability density function (PDF) for selected tracks. The smoothing bandwidth was set to 0.15 μm; the resulting distribution was normal-like. Standard uncertainties associated with expectations $\bar{a}$ and $\bar{b}$ were calculated as $u(\bar{a}) = s(a)/\sqrt{n}$ and $u(\bar{b}) = s(b)/\sqrt{n}$, respectively, where n was the number of selected tracks and $s(a)$ and $s(b)$ were sample standard deviations. The covariance $u(\bar{a},\bar{b})$ was calculated as $u(\bar{a},\bar{b}) = cov(a,b)$, where $cov(a,b)$ was the sample covariance.

3.3. Uncertainty of the parameter B

The uncertainty $u(B)$ arising from the randomness of the number and size of tracks produced by the spontaneous decay of ^{252}Cf was estimated by applying the read-out procedure on the $D_{19},\ldots,D_{41}$ detectors. Each detector was irradiated with fission products of ^{252}Cf. Then the detectors were etched together in the same bath using standard processing conditions described in Section 3.1. Thus, differences between etching conditions (temperature, concentration) did not contribute to the value of $u(B)$. During the read-out procedure, only tracks from perpendicularly impinging fragments ($b/a \geq 0.9$) were analysed. The distribution of fission fragments with respect to mass number should contain two peaks corresponding to light and heavy fragments [28]. These peaks were observed in the Gaussian kernel density estimate of PDF, see Fig. 3, when tracks from all 23 detectors were analysed. For individual detectors, however, the number of tracks from heavy fragments was too small (from 2 to 10, the average was 6.08) to separate the peaks by locating the saddle point. In this case, the classification was based on operator's experience; the largest tracks were marked as produced by the heavy fragments. Fig. 3 shows that this method led to a slight overlap between tracks from light and heavy fragments.

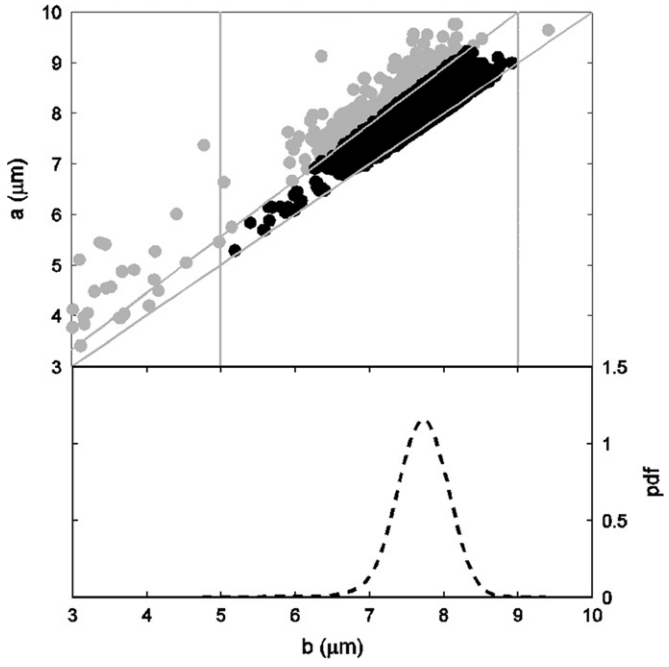

Fig. 2. Determination of parameters a and b. Top: scatter plot of measured major, a, and minor, b, axes for all etched tracks (grey and black markers) and tracks selected for further processing (black markers) created by perpendicularly impinging 400 MeV/u carbon ions. The grey lines stand for selected intervals according to text. Bottom: corresponding PDF estimate for the selected tracks.

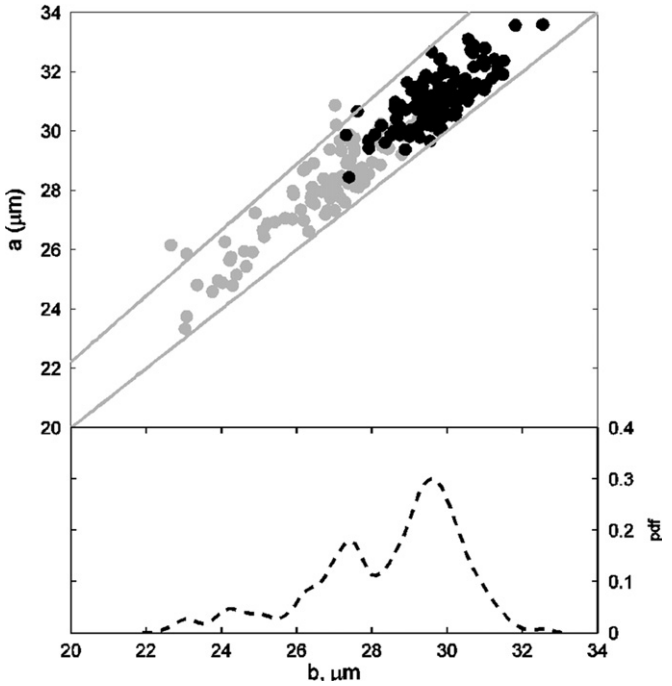

Fig. 3. Determination of B via tracks of fission fragments of ^{252}Cf. Top: scatter plot of track parameters a and b for all tracks (grey and black markers) and tracks from perpendicularly impinging fission fragments ($b/a > 0.9$) selected by the operator (black markers). Bottom: PDF of the parameter b had two major peaks: the left one for light and the right one for heavy fission fragments.

3.4. LET spectrum

For each track, values of V were calculated from Eq. (1) and log-transformed according to $\nu = \lg(V)$. Corresponding values of the log-transformed L denoted as $\lambda = \lg(L/L_0)$, where $L_0 = 1$ keV μm^{-1}, were taken from the calibration curve. Values of λ were histogrammed using 10 equidistant bins in log-transformed coordinates covering the LET range from 7 to 300 keV μm^{-1}. Correction for the critical angle was not done for the sake of simplicity. For each bin, the uncertainty u_1 associated with the randomness of particle detection was calculated from Eq. (3), and the uncertainty u_2 associated with the calibration curve was calculated from Eq. (4) where L was replaced with λ. For simplicity, the uncertainty u_3 was not evaluated, only the difference between bin content of the "original" and smeared-out spectrum was calculated. It was assumed that the "original" spectrum was given by the kernel density estimate of the PDF of λ. This function was smeared-out using the kernel equation (6) in log-transformed coordinates;

symbols L and L' in Eq. (6) were replaced with λ and λ', respectively.

4. Results and discussion

4.1. Uncertainty of the etched out layer B

Sample mean and sample standard deviation of B determined via the method described in Section 3.3 were 29.72 μm and 0.56 μm, respectively; relative standard uncertainty was $u(B)/B = 1.9\%$. We recall that this value does not reflect batch to batch variations, variations arising from differences in etching conditions (temperature, concentration, time, ageing changes etc.), and a possible bias of the fission fragment method. Long-term relative standard uncertainty resulting from calibration detectors $D_1,\ldots,D_{18}$ was 8.5%. This result showed that the uncertainty in B arising from differences in etching conditions was substantially larger than the uncertainty arising from the randomness of detection of fission fragments. The former cannot, however, be used in the formula (A.1) without considering covariances $u(\overline{a},\overline{B})$ and $u(\overline{b},\overline{B})$.

4.2. Uncertainty of the etch rate ratio V

The etch rate ratio $\overline{V}$, associated combined uncertainties $u_c(\overline{V})$ *and* $u_c(V)$, and relative uncertainties $u_{rel} = u_c/\overline{V}$, for tracks from perpendicularly impinging heavy ions with specific values of LET are listed in Table 2. These values were used for the construction of the calibration curve. The relative uncertainty $u_{rel}(\overline{V})$ ranged from 0.56 to 11.41%, with a trend of larger relative uncertainties associated with larger $\overline{V}$ values. Exceptions to this trend were due to the fact that the uncertainty of $\overline{V}$ also depended on the fluence of heavy ions impinging on the detector. Relative uncertainties of $\overline{V}$ larger than 10% are not exceptional, for instance Facius and Horwacik [29] reported differences of up to 25%.

4.3. Calibration curve

The third degree polynomial fitting calibration points in log-transformed coordinates and corresponding confidence intervals for the 95% level are in Fig. 4. Piecewise linear fits are also shown to demonstrate that the confidence intervals depend on the fitting model. The data are in good agreement with measurements of restricted energy loss at the detector surface as a function of the etch rate V by Dörschel et al. [15]. The curves show the same saturation behaviour at higher LET values, which indicates the possible underestimation of V.

Table 2
Etch rate ratio, $\overline{V}$, associated combined uncertainties, u_c, and relative uncertainties, u_{rel}, for tracks from heavy ions with specific values of LET.

L, (keV μm^{-1})	$\overline{V}$	$u_c(\overline{V})$	$u_{rel}(\overline{V})$ (%)	$u_c(V)$	$u_{rel}(V)$ (%)
10.85	1.1578	0.0065	0.56	0.0152	1.31
11.94	1.1858	0.0077	0.65	0.0164	1.39
13.06	1.1891	0.0076	0.64	0.0196	1.65
14.16	1.2278	0.0093	0.76	0.0216	1.76
15.89	1.2190	0.0089	0.73	0.0210	1.72
18.76	1.3029	0.0132	1.01	0.0240	1.84
23.53	1.4246	0.0182	1.28	0.0349	2.45
28.64	1.5068	0.0225	1.49	0.0427	2.83
31.23	1.4731	0.0221	1.50	0.0330	2.24
31.45	1.4762	0.0223	1.51	0.0340	2.31
32.86	1.4622	0.0215	1.47	0.0339	2.32
36.05	1.6010	0.0276	1.73	0.0461	2.88
56.75	1.7309	0.0310	1.79	0.0413	2.39
61.30	1.9142	0.0412	2.15	0.0532	2.78
88.59	2.3231	0.0684	2.94	0.0858	3.69
197.58	3.5073	0.2112	6.02	0.2801	7.98
232.00	4.6101	0.3804	8.25	0.5597	12.14
320.00	6.1918	0.7066	11.41	0.9500	15.34

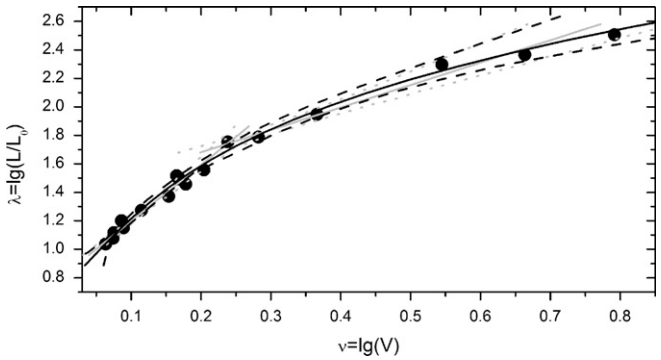

Fig. 4. Measured data and fitted curves $\lambda = f^{-1}(\nu)$ for the third degree polynomial (black thin solid line) and piecewise linear (grey thick solid line) fits and corresponding 95% confidence intervals (black dashed and grey dotted lines). Both fitting models used log-transformed coordinates of $\overline{V}$ and L.

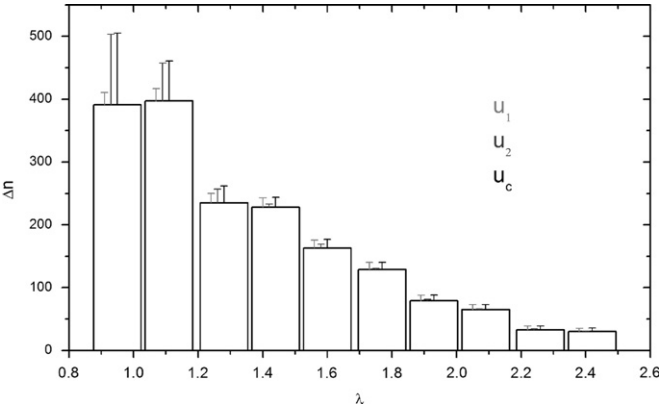

Fig. 5. Histogram of LET values for all detected particles. Uncertainty arising from the randomness of particle detection, u_1, uncertainty arising from the uncertainty of the calibration curve, u_2, and the combined uncertainty, u_c, are shown for each bin.

Table 3
Uncertainty of bin counts for the measured LET spectrum. Linear energy transfer L, the parameter λ, the number of counts in the bin, Δn, relative uncertainty arising from the randomness of particle detection $u_{1,rel}$ relative uncertainty arising from the uncertainty of the calibration curve $u_{2,rel}$ and the relative combined uncertainty $u_{c,rel}$ are listed for each bin. $\Delta\lambda$ was 0.16.

Bin	L, (keV μm^{-1})	λ	Δn	$u_{1,rel}$ (%)	$u_{2,rel}$ (%)	$u_{c,rel}$ (%)
1	8.5	0.93	391	5.1	28.8	29.2
2	12.3	1.09	397	5.0	15.3	16.1
3	18.2	1.26	235	6.5	9.4	11.4
4	26.3	1.42	228	6.6	2.3	7.0
5	38.0	1.58	163	7.8	3.7	8.7
6	56.2	1.75	129	8.8	1.1	8.9
7	81.3	1.91	79	11.3	2.9	11.6
8	117.5	2.07	65	12.4	1.5	12.5
9	173.8	2.24	33	17.4	3.0	17.7
10	251.2	2.40	30	18.3	3.8	18.6

4.4. LET spectrum measured in space

The LET spectrum measured by the detector D_0 positioned in space is in Fig. 5 and summarised in Table 3. The number of detected tracks per unit area was 3×10^4 cm^{-2}. About 70% of these tracks fell in first four bins of the histogram; the corresponding

LET was less than 30 keV μm^{-1}. Relative uncertainty associated with randomness of particle detection u_1 varied from 5.1 to 18.3%, relative uncertainty of calibration varied from 1.1 to 28.8%, and relative combined uncertainty varied from 7.0 to 29.2%.

5. Conclusion

A model for the calculation of measurement uncertainty associated with the number of tracks in a bin of an LET spectrum was developed. The model was applied to a spectrum measured with a track-etched detector in space. For some spectrum bins, the largest contribution to the combined uncertainty was due to the uncertainty associated with the randomness of particle detection. For the others it came from the uncertainty of the calibration curve. Contribution from the cross talk between bins was small for most of the bins as the width of the bins was relatively large compared to the intrinsic resolution of the track-etched detector. The analysis showed that sources of uncertainties other than the randomness of particle detection should not, in general, be neglected.

Acknowledgements

The authors are grateful to colleagues from HIMAC facility. The work was supported by grants GACR 205/09/0171, IAA 100480902 ASCR, GAAV KJB100480901, GACR 202/09/H086 and SGS 10/212/OHK4/2T/14, and bilateral agreement between Czech and Russian Academy of Sciences.

Appendix A

The law of propagation of uncertainty

The Guide to the expression of uncertainty in measurement (GUM) [27] introduces a framework for the calculation of uncertainty associated with the quantity Y that depends on K input quantities $X_1,\ldots,X_K$ via a functional relationship $Y=f(X_1,\ldots,X_K)$. The combined uncertainty $u_c(y)$ associated with Y is evaluated at the value of $y=f(x_1,\ldots,x_K)$, where $x_1,\ldots,x_K$ are the expectations of $X_1,\ldots,X_K$, as [27]

$$u_C^2(y)=\sum_{i=1}^{K}\left(\frac{\partial f}{\partial x_i}\right)^2 u^2(x_i)+2\sum_{i=1}^{K-1}\sum_{j=i+1}^{K}\frac{\partial f}{\partial x_i}\frac{\partial f}{\partial x_j}u(x_i,x_j) \tag{A.1}$$

where $u(x_i)$ are uncertainties associated with X_i, and $u(x_i, x_j)$ are covariances associated with X_i and X_j, $1\le i,j\le K$. Partial derivatives are evaluated at the expectations $x_1,\ldots,x_K$; they are called sensitivity coefficients as they express the sensitivity of the quantity Y on the input quantities $X_1,\ldots,X_K$. For normally distributed input variables and well behaved functions f, the distribution of Y is t-or normal-like. A coverage interval for Y is then given by the expanded uncertainty ku_c as $y\pm ku_c$, where the coverage factor k corresponds to a given coverage level. For instance $k=2$ corresponds to 95% coverage level for a normal-like distribution.

Uncertainty of the etch rate ratio V

Let $\alpha=\overline{a}/\overline{B}$ and $\beta=\overline{b}/\overline{B}$ be the expected major and minor axes of the etched track, respectively, relative to the expected removed layer $\overline{B}$. Then Eq. (1) can be written for the expected etch rate ratio $\overline{V}$ as

$$\overline{V}=\left[\text{sinarctan}\left(\frac{1-\beta^2}{2\alpha}\right)\right]^{-1}=\frac{\sqrt{4\alpha^2+(1-\beta^2)^2}}{1-\beta^2} \tag{A.2}$$

It can be shown that sensitivity coefficients c_1, c_2 and c_3 of the functional relationship $\overline{V}=\overline{V}(\overline{a},\overline{b},\overline{B})$, see Eq. (A.1), are

$$c_1\equiv\frac{\partial\overline{V}}{\partial\overline{a}}=\frac{4\alpha}{\overline{B}(1-\beta^2)^2}\frac{1}{\overline{V}} \tag{A.3}$$

$$c_2\equiv\frac{\partial\overline{V}}{\partial\overline{b}}=\frac{2\beta}{\overline{B}(1-\beta^2)}\left(1-\frac{1}{\overline{V}}\right) \tag{A.4}$$

$$c_3\equiv\frac{\partial\overline{V}}{\partial\overline{B}}=\frac{-4\alpha^2(1+\beta^2)}{\overline{B}(1-\beta^2)^3}\frac{1}{\overline{V}} \tag{A.5}$$

The combined uncertainty $u_c(\overline{V})$defined by Eq. (A.1) is then

$$u_C^2(\overline{V})=[c_1u(\overline{a})]^2+[c_2u(\overline{b})]^2+[c_3u(\overline{B})]^2+2c_1c_2u(\overline{a},\overline{b})+2c_1c_3u(\overline{a},\overline{B})+2c_2c_3u(\overline{b},\overline{B}) \tag{A.6}$$

where $u(\overline{a})$, $u(\overline{b})$, and $u(\overline{B})$ are standard uncertainties associated with expectations $\overline{a}$, $\overline{b}$, and $\overline{B}$, respectively, and $u(\overline{a},\overline{b})$, $u(\overline{a},\overline{B})$, and $u(\overline{b},\overline{B})$ are corresponding covariances.

References

[1] F. Spurný, Radiation Physics and Chemistry 61 (3–6) (2001) 301.
[2] E.V. Benton, Advances in Space Research 6 (11) (1986) 315.
[3] D. Nikezic, K.N. Yu, Materials Science and Engineering: R 46 (2004) 51.
[4] R.J. Tanner, D.T. Barlett, L.G. Hager, Radiation Measurements 40 (2005) 549.
[5] A.N. Golovchenko, J. Skvarć, R. Ilić, L. Sihver, V.P. Bamblevski, S.P. Tretyakova, D. Schardt, R.K. Tripathi, J.W. Wilson, R. Bimbot, Nuclear Instruments and Methods 159 (4) (1999) 233.
[6] E.R. Benton, C.E. Johnson, J. DeWitt, N. Yasuda, E.V. Benton, M.H. Moyers, A.L. Frank, Radiation Measurements 46 (5) (2011) 527.
[7] ICRP, Recommendations of the International Commission on Radiological Protection, 60, ICRP Publication, 1991.
[8] K. Pachnerová Brabcová, I. Ambrožová, F. Spurný, Radiation Protection Dosimetry 143 (2–4) (2011) 440.
[9] E.J. Hall, A.J. Giaccia, Radiobiology for Radiologist, third ed., Lippincott, Philadelphia, 1988.
[10] R.L. Fleischer, P.B. Price, R.M. Walker, Nuclear Tracks in Solids: Principles and Applications, Universtity of California Press, 1975.
[11] P. Wuhnsen, W. Enge, R. Beaujean, Nuclear Tracks and Radiation Measurements 8 (1–4) (1984) 179.
[12] S.K. Chakarvarti, N. Lal, K.K. Nagpaul, European Journal of Physics 1 (1980) 133.
[13] Z.-F. Ibrahimi, C.B. Howarth, J.C.H. Miles, Radiation Measurements 44 (2009) 750.
[14] D. Nikezic, K.N. Yu, Nuclear Instruments and Methods A 450 (2000) 568.
[15] B. Dörschel, D. Hermsdorf, K. Kadner, S. Starke, Radiation Measurements 35 (3) (2002) 287.
[16] S. Kodaira, N. Yasuda, N. Hsebe, T. Doke, S. Ota, K. Ogura, Nuclear Instruments and Methods A 547 (1) (2007) 163.
[17] S.A. Durrani, R.K. Bull, Solid State Nuclear Track Detection, Pergamon Press, 1987.
[18] D. Nikezic, K.N. Yu, Materials Science and Engineering R 46 (2004) 51.
[19] F. Membrey, M. Fromm, A. El Rahamany, A. Chambauder, Nuclear Tracks and Radiation Measurements 21 (3) (1993) 417.
[20] F. Spurný, J. Bednář, L. Johansson, A. Sätherberg, Radiation Measurements 26 (5) (1996) 645.
[21] E.R. Benton, Radiation Dosimetry at Aviation Altitudes and in Low-Earth Orbit, Thesis, Department of Experimental Physics, National University of Ireland, 2004.
[22] K. Pachnerová Brabcová, Study and Development of Track Etch Detectors for Dosimetric Purposes, Thesis, Czech Technical University in Prague.
[23] N. Lal, Y.P. Mehta, A.K. Thakur, S. Kumar, Nuclear Tracks and Radiaton Measurements 17 (4) (1990) 599.
[24] N. Yasuda, K. Namiki, Y. Honma, Y. Umeshima, Y. Marumo, H. Ishii, E.R. Benton, Radiation Measurements 40 (2005) 311.
[25] T. Kanai, M. Endo, S. Minohara, N. Miyahara, H. Koyama-ito, H. Tomura, N. Matsufuji, Y. Futami, A. Fukumura, T. Hiraoka, Y. Furusawa, K. Ando, M. Suzuki, F. Soga, K. Kawachi, International Journal of Radiation Oncology 44 (1) (1999) 201.
[26] J.F. Ziegler, J.P. Biersack, M.D. Ziegler, SRIM: The stopping and range of ions in matter, Pergamon Press, New York, 2008.
[27] JCGM 100:, Evaluation of Measurement Data—Guide to the expression of uncertainty in measurement, Geneva, Switzerland, 2008.
[28] L.E. Glendenin, E.P. Steinberg, Journal of Inorganic and Nuclear Chemistry 1 (1–2) (1955) 45.
[29] R. Facius, T. Horwick, Three dimensional determination of etch track parameters in plastic nuclear track detectors: findings on bulk etch rate and implications for dosimetry, 13th WRMISS, Krakow, Poland, 2006.